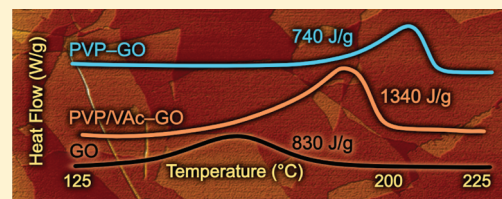# *In Situ* Reduction of Graphene Oxide in Polymers

A. Jaeton Glover,[†,‡] Minzhen Cai,[†] Kyle R. Overdeep,[‡] David E. Kranbuehl,[‡] and Hannes C. Schniepp[*,†]

[†]Department of Applied Science, The College of William & Mary, Williamsburg, Virginia 23187, United States

[‡]Department of Chemistry, The College of William & Mary, Williamsburg, Virginia 23187, United States

Ⓢ *Supporting Information*

**ABSTRACT:** *In situ* reduction of graphene oxide (GO) at moderate temperatures within a polymer was observed using differential scanning calorimetry (DSC). Comparison of heats of reduction from DSC data in poly(vinylpyrrolidone), poly(vinyl acetate), and poly(vinylpyrrolidone/vinyl acetate) nanocomposites demonstrates that the polymer chemistry strongly influences the extent of reduction. These results are compared to the time−temperature relationship for GO reduction in air and in dimethylformamide at the same temperatures, determined through changes in the atomic carbon-to-oxygen ratio. GO reduction was independently confirmed by electrical conductivity and optical absorption measurements, as well as Raman spectroscopy. These results show that GO sheets are reduced depending on the time−temperature history and polymer chemistry at the particles' location. For nanocomposites this can lead to improvement or reduction of desired properties and is thus pertinent to thermal processing of polymer nanocomposites based on functionalized graphene.

## ■ INTRODUCTION

Interest in the incorporation of chemically derived single-layer graphene or functionalized graphene into polymers has become increasingly widespread[1−10] due to its outstanding mechanical properties,[11,12] good electrical conductivity,[11] high surface area,[13] impermeability to gases,[2] and low cost. Nanocomposites based on these materials feature significant property improvements when less than 1% of nanoparticles based on single-layer graphene are added.[1] The common means of obtaining these particles is through exfoliation of graphite oxide, which is the product of native graphite treated with the Hummers method.[14,15] The oxidized graphite is readily exfoliated mechanically[4] or thermally,[13,16] into single-layer sheets. This process is economical in terms of cost and scale.

Because of the addition of hydroxyl, epoxide, and carboxylic acid surface groups during the Hummers reaction,[17] graphene oxide (GO), the single-layer form of graphite oxide, is hydrophilic (polar) and easily disperses in water and many organic solvents that are used for polymer processing, such as dimethylformamide (DMF)[18] and n-methylpyrrolidone (NMP),[19,20] which allows facile production of graphene−polymer nanocomposites.[1−4] The functional groups of GO can subsequently be removed chemically[4] or thermally;[13] the resulting material, reduced GO, features distinctly different electronic and interfacial properties.[4] This reduction increases the atomic carbon-to-oxygen (C:O) ratio,[13] which is about 2 in GO. With increasing C:O ratio, the bandgap of GO becomes smaller,[21,22] reaching zero in perfect graphene. Conductivity has been observed in GO with a C:O ratio of 10 or more.[13,23,24] Reduction also renders the GO sheets more hydrophobic (nonpolar). On one hand, an increased hydrophobicity significantly affects the interaction of the sheets with solvents, so that obtaining good dispersions becomes increasingly

difficult. On the other hand, the change in surface polarity changes the sheets' interaction with polymers, which is expected to have a significant impact on the mechanical properties of the polymer nanocomposites.

The focus of this work is to demonstrate that GO undergoes thermal reduction during thermal processing of a polymer nanocomposite. We show that the extent of this reduction varies with the time and temperature of processing and the chemical structure of the polymer. Our findings show that poly(vinylpyrrolidone) (PVP) inhibits, whereas poly(vinylpyrrolidone/vinyl acetate) (PVP/VAc), and to a greater degree, poly(vinyl acetate) (PVAc) facilitates the reduction of GO *in situ* at temperatures below 250 °C. PVP and PVP/VAc are particularly attractive due to their water solubility, making them compatible with aqueous GO dispersions. Consequently, these nanocomposites can be manufactured on the basis of water as a solvent only, avoiding the use of organic solvents that are much more problematic with respect to environmental considerations. We report the *in situ* reduction of GO in five different PVP, PVAc, and PVP/VAc polymer matrices, verified by thermal techniques, conductivity measurements, optical characterization, and Raman spectroscopy. We compare our results to the time−temperature dependence of reduction of GO *in air* in terms of C:O ratio at temperatures up to 250 °C. The change in the C:O ratios of the reduced products determined by elemental analysis are thereby quantified for the first time as a function of temperature, time and solvent.

Clearly, these changes in the C:O ratio will affect the properties of the nanocomposites, as the sheets' electronic properties, as
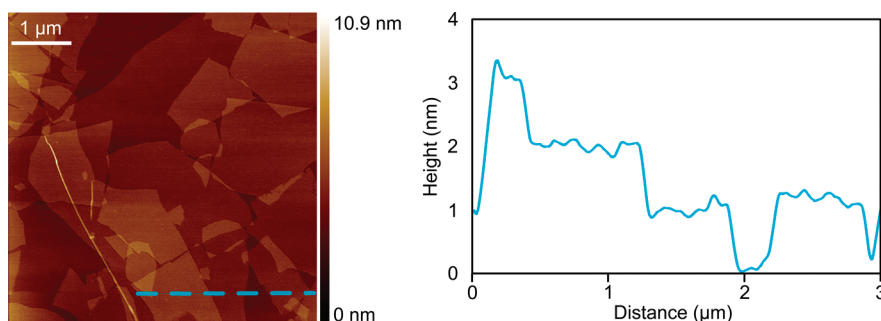
**Figure 1.** Contact mode atomic force microscopy scan (left) and cross-section (right) of single-layer GO sheets (position of cross-section in the image indicated by light blue, dashed line). Typical sheet width is one micrometer, and thickness one nanometer. Heights of more than 1 nm in the cross-section are a result of overlapping single-layer sheets due to high area density of sheets in this sample.

well as their mechanical interactions with the polymer are altered. This phenomenon may result in degradation, or it could be used to intentionally enhance the desired properties of the nanocomposite. For instance, the controlled bulk reduction of GO in a polymer nanocomposite allows systematic fine-tuning of the material's band gap, conductivity and mechanical properties.[25] Via controlled, localized GO reduction across a nanocomposite, patterns or gradients of desired bandgap, conductivity, or mechanical properties can be "written" into the material in a simple way;[25] similar properties cannot be easily achieved by other methods.

In order to provide an overview and a comparison to existing approaches, the common GO reduction procedures involving the use of either chemical reducing agents or heat are reviewed. Reduction by chemical reagents includes exposure to hydrazine,[15,18,26−34] dimethylhydrazine,[4] sodium borohydrate,[35] hydroquinone,[36] alkaline conditions,[37] ascorbic acid,[38,39] trioctylphosphine,[40] glucose,[41] tyrosine-rich proteins,[42] aluminum powder in acidic conditions,[43] and gaseous $H_2$.[44] Chemical reduction is effective at moderate temperatures (<100 °C), but involves considerable care, multiple steps, and some of the reagents are toxic.[15,18,26−34]

Thermal reduction is another means of reduction. Schniepp et al. have demonstrated simultaneous reduction and exfoliation in argon via tube furnace at 1050 °C.[13] This method was further characterized by McAllister et al., who determined that exfoliation occurs at temperatures of 550 °C and above, where production of gaseous products—primarily $H_2O$ and $CO_2$—by decomposition of oxygen-containing functional groups outpaces the escape of products by diffusion.[16] Wang et al. reported reduction of GO from 550 to 1100 °C under Ar and $H_2$.[45] GO reduction has also been demonstrated under vacuum at temperatures ranging from 140−300 °C and 600−800 °C.[46,47] Li et al. discuss simultaneous N-doping and thermal reduction at 300 °C and above under $NH_3$.[48]

Localized thermal reduction has been demonstrated by a heated AFM probe.[25] Further, Cote et al. report a photothermal method for GO reduction whereby a xenon flash generates the heat necessary to catalyze reduction.[49] Electron transfer from $TiO_2$ irradiated by UV light to suspended GO particles has been shown by Williams et al.[50]

Expanding upon thermal reduction work, Liao et al. describe the reduction of GO dispersed in water (solvothermal reduction) at 95 °C and ambient pressure.[51] Nethravathi and Rajamathi describe solvothermal reduction methods in water, ethanol, butanol, and ethylene glycol in sealed vessels at temperatures ranging from 120 to 200 °C.[52] Maximum reduction is met in all solvents at 16 h, and C:O ratios vary with solvent type from 6 to 21.[52] Solvothermal reduction at atmospheric pressure by refluxing GO in NMP at 205 °C for 24 h yielded a C:O ratio of 5.[19,20] Chen and Yan report partial reduction of GO at 150 °C, atmospheric pressure, in $DMAc/H_2O$ (10:3 v/v) for 1 h and complete reduction at 5 h.[53] Similarly, a GO dispersion in 6:1 $DMAc/H_2O$ reduced by 800 W microwave led to partial reduction in 3 min and total reduction in 10 min.[54] Zhou et al. report reduction under pressure of GO dispersed in water at 150 °C and more so at 180 °C for 6 h.[55] GO dispersed in propylene carbonate has been reduced at 150 °C for 12 h.[56] Recently, Lin et al. have described the solvothermal reduction of GO in water at 100 °C and DMF at 150 °C.[57] Their results show that reduction in DMF leads to a greater C:O ratio than GO reduced at the same temperature in air, supporting the conclusion reached by Nethravathi and Rajamathi that the degree of reduction is solvent-dependent.[52]

In spite of all the literature available regarding the reduction of GO, the time−temperature dependence on the reduction of GO in air at low temperatures (150−250 °C) has yet to be determined in terms of quantifying the effect on the C:O ratio. In this work we elucidate the time−temperature dependence of GO reduction in air and in DMF, and we show for the first time that the C:O ratio of GO within a polymer matrix increases during processing by an amount which depends on the chemistry of the polymer used and the processing history.

## ■ MATERIALS AND METHODS

GO was produced using the Hummers method.[14] The material was exfoliated acoustically using a Microson XL2007 tip sonicator (Microson, Farmingdale, NY) with a power of 100 W either in ultrapure water (Millipore Synergy ultrapure water system, Millipore, Billerica, MA) at 2 mg/mL, or in DMF (Sigma-Aldrich, anhydrous, 99.8%) at 1 mg/mL. The obtained dispersions did not contain any visible microparticles and were stable for days. The degree of GO exfoliation was further evaluated by atomic force microscopy (AFM). The aqueous GO dispersions were, therefore, diluted to a concentration of 0.1 mg/mL and spin-coated onto freshly cleaved mica substrates and scanned in contact mode using an NT-MDT NTEGRA Scanning Probe Laboratory (Zelenograd, Moscow, Russia). A SiNi triangular cantilever (spring constant 0.27 N/m, tip radius of curvature <15 nm) from BudgetSensors (Sofia, Bulgaria) was used. A representative scan and cross-section are shown in Figure 1. Typical sheet width was on the order of 1 $\mu$m; the thickness of virtually all sheets was around 1 nm, indicating complete exfoliation into single-layer material.
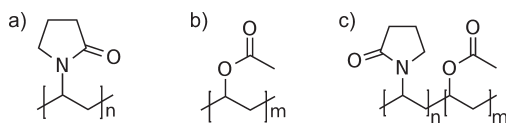
a) b) c)

**Figure 2.** Structures of (a) poly(vinylpyrrolidone) and (b) poly(vinyl acetate) and (c) poly(vinylpyrrolidone/vinyl acetate).

**Table 1. Polymer Name, Fikentscher K-Value, and Calculated Viscosity-Average Molecular Weight[a]**

| polymer name | Fikentscher K-value | $M_v$ (g/mol) |
|---|---|---|
| C-17 | 17 | 2900 |
| K-29/32 | 31* | 8810 |
| K-120 | 120 | 173 000 |
| S-630 | 40* | 15 100 |

[a] Items with an asterisk (∗) denote use of an average when K-value ranges were given.

Thermogravimetric analysis (TGA) experiments were conducted on a TA Instruments Q-500 (New Castle, DE) using a platinum pan and were purged with nitrogen. DSC experiments were conducted on a TA Instruments MDSC 2920 using aluminum hermetic pans sealed in air. The temperature ramps were 1 °C/min from room temperature to 250 °C.

In order to establish the time−temperature reduction behavior of GO in air, TGA and DSC characterization was carried out. In addition, GO was also heated and held at different temperatures for 10 min and for 4 h and subsequently tested via elemental analysis (Galbraith Laboratories, Inc., Knoxville, TN) to determine the C:O ratio. The GO samples for these studies were prepared by redrying aqueous GO suspensions under vacuum at 45 °C for 24 h prior to use. This procedure was used to allow byproducts to escape, so that the C:O ratio could be determined based solely upon the covalently bound oxygen. Solvothermal reductions were carried out using the 1 mg/mL GO−DMF dispersions. Reduction was performed in a model 452HC pressure vessel (Parr Instrument Company, Moline, IL) in a temperature controlled silicone oil bath. Upon cooling, the material was dried under vacuum at 50 °C for 24 h. Elemental analysis was carried out subsequently.

The PVP (C-17, K-29/32 and K-120) and PVP/VAc (S-630) polymers used in the nanocomposites were provided by International Specialty Products (Wayne, NJ). Their structures are shown in Figure 2. The C- and K- designations for the PVP refer to the Fikentscher "K" value, a representation of the viscosity of the polymer that increases with average molecular weight.[58,59] The K values were converted to viscosity-average molecular weights, $M_v$, shown in Table 1, and will henceforth be referred to by their $M_v$ values. The S-630 PVP/VAc is a 60:40 by weight PVP:VAc copolymer with a K-value between 30 and 50.[60] The PVAc polymer has a MW of 140,000 (140 K PVAc) and was purchased from Sigma-Aldrich.

In order to make GO−polymer nanocomposites, solid polymer was dissolved in GO dispersions, and the solution was then cast in film form. The solvent was subsequently evaporated by drying at room temperature in air for 1 week. For the PVP and PVP/VAc polymers, the 2 mg/mL aqueous GO dispersion was used; the dried films contained less than 5% water, as determined by TGA. For PVAc the 1 mg/mL dispersion of GO sheets in DMF was used, as PVAc is not water-soluble. The obtained GO−PVAc films were dried under vacuum at 40 °C. Since the boiling point of DMF is within the temperature range of GO reduction, TGA mass loss data alone could not be used to determine solvent content data accurately. However, evidence of residual solvent did not appear in the DSC thermogram, and the heat released by GO reduction increased to a steady value within 2 weeks.
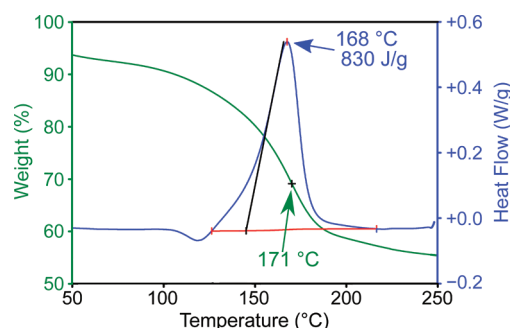


**Figure 3.** TGA data (green) of GO reduction indicating a maximum rate of mass loss at 171 °C. DSC data (blue) of GO reduction indicates a maximum heat loss at 168 °C and a release of 830 J/g.

Electrical conductivity measurements were carried out using a gold interdigitated dielectric sensor deposited on Kapton film for unheated and heated composites of all three polymer matrices containing 9.1% GO. Details of this measurement are described in the Supporting Information. For optical absorption measurements samples of all three polymers were manufactured with a GO loading of 1% by mass, a concentration yielding sufficiently transparent films. For each matrix material a sample was cut into two pieces and one of the pieces was subjected to heating. This procedure was chosen to ensure the observed differences were due to heating and not due to differences in sample preparation. A He−Ne laser with a wavelength of 633 nm was used to characterize optical absorption. The beam was attenuated to a power of 2 mW and collimated with a diameter of 3 mm. Unheated and heated composite sheets were placed in the beam; optical power of the transmitted beam was measured using a power meter, Thermo Oriel model 70260 (Stratford, CT), and compared to the power of the beam before entering the composite. Readings were taken for at least five different beam positions on each sample in order to average over sample inhomogeneities. The same optical transmission measurements were carried out for each of the neat polymers without and with heat treatment. These control measurements were done to demonstrate that heating mainly changed the optical properties of GO and not the properties of the polymer matrices. Raman spectra from samples of unheated and heated 9.1% PVAc−GO composites were taken using a Renishaw (Gloucestershire, U.K.) inVia Raman microscope with a 633 nm He−Ne laser and a 100× objective (0.9 N.A.); spectra were collected from 100 to 4000 cm$^{-1}$. Three spectra were collected at different areas of each sample and averaged to improve the signal-to-noise ratio. The neat polymer and composite samples used to show thermally induced changes in electrical conductivity, optical absorption, and Raman spectra were heated using the TGA furnace for best temperature accuracy.

## ■ RESULTS AND DISCUSSION

**1. Reduction in Air.** DSC experiments with pure GO were conducted in air; Figure 3 establishes a baseline for later comparison with GO reduced in DMF and in nanocomposites made with PVP, PVP/VAc, and PVAc. The DSC data reveals an exothermic event occurring between 125 and 220 °C. This event reaches a peak at 168 °C, and integration of the peak gives a caloric value of 830 J/g of GO. The endothermic event at 120 °C is due to vaporization of residual water. The TGA data, also plotted, shows a 31% mass loss in the 125 to 220 °C range corresponding to the exothermic DSC peak. The highest rate of mass loss, indicated by a first derivative maximum, occurred at 171 °C. These results agree with work done by McAllister et al. in that both the exothermic event and the peak rate of weight loss
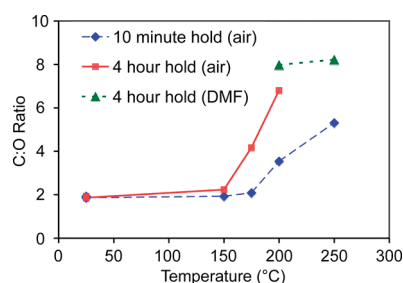
**Figure 4.** Change in C:O ratio of GO with respect to temperature and hold time in air for 10 min (blue, dashed), in air for 4 h (red, solid), and in DMF for 4 h (green, dotted).



**Figure 5.** TGA data for neat 173 K PVP (blue) showing a mass loss of 0.3% at 250 °C and the 173 K PVP—9.1% GO composite (green) indicating a 2.76% difference in mass at 250 °C.

**Table 2. C:O ratio of GO as a Function of Reduction Time and Temperature**

| temp (°C) | exposure time | environment | C content (%) | O content (%) | atomic C:O ratio |
|---|---|---|---|---|---|
| 25 | - | - | 56 | 39 | 1.9 |
| 55 | 4 months | water | 63 | 27 | 3.2 |
| 150 | 10 min | air | 56 | 39 | 1.9 |
| 150 | 240 min | air | 60 | 36 | 2.2 |
| 175 | 10 min | air | 59 | 37 | 2.1 |
| 175 | 240 min | air | 73 | 23 | 4.2 |
| 200 | 10 min | air | 69 | 26 | 3.5 |
| 200 | 240 min | air | 81 | 16 | 6.8 |
| 200 | 240 min | DMF | 72 | 12 | 8.0 |
| 250 | 10 min | air | 80 | 20 | 5.3 |
| 250 | 240 min | DMF | 73 | 12 | 8.2 |

occur at approximately the same temperature.[16] However, our results indicate these events occur 30 °C lower than temperatures reported by McAllister et al.[16] Since our temperature ramp rates are the same as in work by McAllister et al. (1 °C/min), this is likely due to differences in the GO used, as the McAllister GO was produced by the Staudenmaier method instead of the Hummers method.[16]

In order to further analyze the time—temperature behavior of this process we heated GO to temperatures of 150, 175, 200, and 250 °C, and held it at these temperatures for 10 min and for 4 h. The C:O ratio of the resulting materials was determined via elemental analysis. The results are shown in Figure 4; the numerical values of the results are shown in Table 2. These data reveal that up to 150 °C only a slight reduction (increase of the C:O ratio) occurs. This is in agreement with our DSC data (Figure 3), where the bulk of the heat is produced at temperatures above 150 °C. Worth noting is that Figure 4 shows a less significant change in the C:O ratio for 150 °C than one would expect by looking at the DSC data, which shows a more significant reduction activity. However, the difference can be explained by the fact that the two scales are not linearly related: a small increase of the C:O ratio above 2 causes a relatively significant mass loss.

**2. Reduction in Liquids.** We carried out solvothermal reduction under pressure in DMF at temperatures of 200 and 250 °C for 4 h; the corresponding data points showing the results of subsequent chemical analysis are included in Figure 4/Table 2. The products held at 200 and 250 °C had C:O ratios of 8.0 and 8.2, respectively, and remained stable dispersions for more than
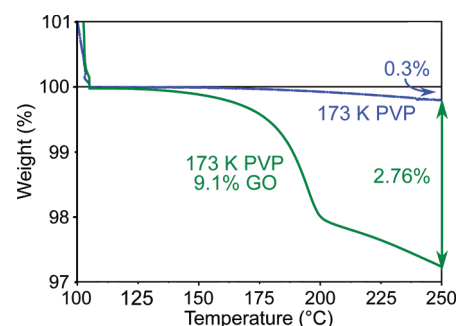
72 h. The 200 °C reduction in DMF yields a higher C:O ratio than what was seen in air, a conclusion in general agreement with previous results by Lin et al.[57] They demonstrate that GO reduced in air at 100 °C for 24 h lost 60% of its mass (through release of oxygen-containing groups) by TGA while GO reduced in DMF at 150 °C for 1 h showed "no rapid weight loss," suggesting a higher degree of reduction.[57] Their mass loss for GO reduced in air is much higher than what we find, which is likely due to their 20 °C/min ramp rate vs our 1 °C/min.[57] Dubin et al. studied solvothermal reduction of GO in NMP, a solvent that is in some respects similar to DMF. They showed that GO refluxed at 205 °C for 24 h in NMP has a C:O ratio of 5.15.[20] It is interesting to compare our results for a 240-min hold at 200 °C in air and in DMF. We find that the material in DMF was more strongly reduced (C:O ratio 8.0 vs 6.8). These findings support the premise that the environment in which the GO is dispersed defines, along with temperature and time of reduction, the degree of reduction. A dependence on the surrounding medium was also observed by Nethravathi and Rajamathi, who showed that the GO reducing power of different solvents decreases in the following order ethylene glycol > ethanol >1-butanol.[52]

To explore the effects of low temperatures over long times on the reduction of GO at even lower temperatures, we dispersed GO sheets in water at 2 mg/mL and held them in a sealed vessel at 55 °C for four months and found a C:O ratio of 3.2 (Table 2). Remarkably, this C:O ratio is even higher than the 3.12 reported by Dubin et al. after refluxing (100 °C) GO in $H_2O$ for 24 h.[20] This demonstrates that even at relatively low temperatures GO can be reduced significantly when enough time is given. The implication from this data is that GO reduces to a point where material properties are altered, even close to room temperature. For GO-based applications, this behavior needs to be taken into account. Our work goes beyond prior reports, as it establishes the time—temperature relationship of GO reduction in different environments.

**3. In Situ Nanocomposite Reduction.** Figure 5 shows the TGA data of a 1 °C/min ramp from room temperature to 250 °C of the neat 173 K PVP (PVP with $M_v$ = 173 000 g/mol) and its composite loaded with 9.1% GO taken under nitrogen atmosphere. The quality of the aqueous GO dispersion used to make the composite was verified to contain only single sheets by AFM. Both materials were dried with a 60-min isotherm at 100 °C and the results were normalized with respect to postdrying masses to counter the effects of different initial water contents in the materials. The neat polymer lost only 0.3% of its mass over the range of the experiment, indicating that it has good thermal stability, as

indicated in Figure 5. In contrast, the nanocomposite containing GO shows a mass loss which is almost 1 order of magnitude larger. As shown in Figure 5, upon reaching 250 °C there is a 2.76% difference in mass loss between the two materials. Given the mass fraction of GO (9.1%), this means that the relative mass loss in the GO is 30.3%. This is in excellent agreement with the mass lost by GO reduced under nitrogen in Figure 3 (31%). This suggests that the mass difference of the nanocomposite is completely due to mass loss of the embedded GO particles.

Figure 6 shows the corresponding DSC data for the 173 K PVP−GO nanocomposite reduction at 1 °C/min. The published $T_g$ of the neat 173 K PVP is faintly visible at 176 °C,[59] and the thermal stability of the neat polymer is demonstrated by the otherwise featureless thermogram. The onset of the reduction of the GO in the 173 K PVP nanocomposite occurs at 165 °C and is completed at 212 °C. The peak of the exotherm occurs at 206 °C, as compared to the peak reduction of GO in air at 168 °C. This shift of the peak reaction temperature toward higher temperatures indicates that the 173 K PVP polymer provides stability to the GO, possibly arising from interfacial interactions between the 173 K PVP and GO. The shift in the baseline over the course of the reduction of the composite is likely due to the $T_g$ of the nanocomposite falling within the temperature range of the reduction. Integration of the reaction energy yields 67.3 J/g for the composite, or 740 J/g for the GO in the 173 K PVP composite. This is significantly lower than the heat of reduction of pure GO, 830 J/g, and further underlines that the GO is stabilized through interfacial interactions with the 173 K PVP.

Table 3 shows similar reaction data for the lower molecular weights of PVP, 2900 (2.9 K PVP) and 8800 (8.8 K PVP) g/mol. All heats of reduction for the PVP−GO composite samples are similarly lower than the heat of reduction of the pure GO,
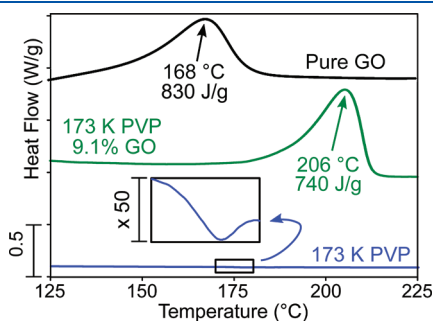
supporting the view that the reduction is hindered by GO−polymer interactions. 173 K PVP, the PVP polymer with the highest molecular weight, features the lowest heat of reduction, which indicates that it stabilizes the GO to a greater degree than the lower molecular weight versions, 2.9 K and 8.8 K, of the PVP polymers. However, the difference is 30−40 $J/g_{GO}$, which is only slightly greater than the error of measurement, 20 $J/g_{GO}$.

The 15.1 K ($M_v$ = 15 100 g/mol) PVP/VAc copolymer system also features excellent thermal stability up to 200 °C, making it suitable for thermal study of *in situ* GO reduction. The DSC of the neat polymer shows a featureless, almost perfectly flat curve (Figure 7). When loaded with 9.1% GO, this polymer shows a heat of reduction of 1340 J/g for the GO in the polymer composite (Figure 7). This value is higher than the three PVP−GO composites, as well as the neat GO. This suggests a higher degree of *in situ* GO reduction is occurring in the PVP/VAc nanocomposite than would be seen in GO's pure form. The peak reduction temperature in the PVP/VAc composite, 192 °C, is higher than that of the pure GO at 168 °C, and lower than that in the PVP composites, whose peak reduction temperatures ranged from 199−206 °C. A similar trend is seen in the onset of reduction temperatures. The PVP/VAc copolymer composite has an onset of reduction of 135 °C, significantly lower than the PVP composites, which range from 160−165 °C. The PVP/VAc copolymer clearly aids the reduction of the GO compared to PVP, which decreases degree of reduction relative to air.

Subsequently, the *in situ* reduction of GO within a 140 K PVAc nanocomposite was studied; the results are shown in Figure 8. The DSC and TGA data for the neat polymer indicate that it is thermally stable through 200 °C. For a 9.1% by mass GO−PVAc composite, the heat of reduction of is 1450 ± 20 $J/g_{GO}$, an increase of 110 $J/g_{GO}$ over the GO−PVP/VAc composite. The peak reduction temperature, 158 °C, was considerably lower than the other composite systems we studied. Likewise, the onset
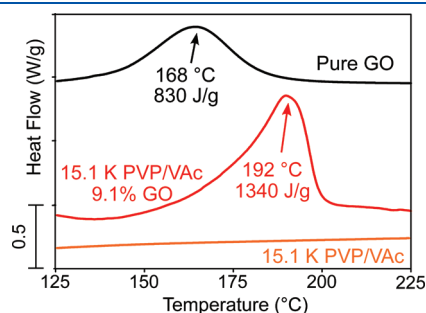


**Figure 6.** DSC thermogram of neat 173 K PVP (blue) and its composite loaded with 9.1% GO (green). A 50× magnification at 176 °C (inset) reveals the $T_g$ of the neat 173 K PVP. The composite exotherm has a maximum at 206 °C and releases 740 J/g in the composite. Pure GO reduced in air is also shown (black) for comparison purposes.



**Figure 7.** DSC thermogram comparing reduction of neat GO (black), 15.1 K PVP/VAc (orange) and 15.1 K PVP/VAc loaded with 9.1% GO (red).

**Table 3. Heat of Reduction Data for PVP, PVP/VAc, and PVAc Composites Loaded with GO[a]**

| material (K denotes KDa) | GO conc. [%] | onset of red. [°C] | peak of red. [°C] | end of red. [°C] | $\Delta H_{red}$ [J/g of GO] |
|---|---|---|---|---|---|
| neat GO | 100.0 | 125 | 168 | 220 | 830 ± 20 |
| 2.9 K PVP−GO | 9.1 | 160 | 199 | 225 | 770 ± 20 |
| 8.8 K PVP−GO | 9.1 | 165 | 203 | 220 | 780 ± 20 |
| 173 K PVP−GO | 9.1 | 165 | 206 | 212 | 740 ± 20 |
| 15.1 K PVP/VAc−GO | 9.1 | 135 | 192 | 220 | 1340 ± 20 |
| 140 K PVAc−GO | 9.1 | 80 | 158 | 178 | 1450 ± 20 |

[a] K denotes the polymer molecular weight $M_v$ in KDa, for example, 173 000 g/mol PVP is referred to as 173 K PVP.
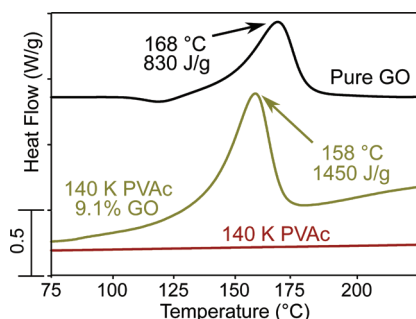
**Figure 8.** DSC thermogram comparing reduction of neat GO (black), 140 K PVAc (dark red) and 140 K PVAc loaded with 9.1% GO (olive).

temperature, 80 °C, is much lower than that seen in the PVP/VAc copolymer composite (135 °C).

Comparing the calorimetric data for nanocomposites made with the different polymers investigated here we find the following trend: for PVP composites we find a decrease of the heat of reduction and an increase in the reaction temperatures with respect to pure GO, suggesting that the presence of PVP hinders the reduction. When a PVP/VAc copolymer is used as the nanocomposite matrix, the reduction temperatures are reduced with respect to the GO–PVP composite. More importantly, the heat of reduction is not only higher than for the GO–PVP system, but even higher than for pure GO. This strongly suggests that the VAc component in this system has the opposite effect than PVP: due to the presence of the vinyl acetate group, the reduction of GO is not hindered but enhanced. This trend is confirmed when GO is embedded in pure PVAc, where the heat of reduction is further increased and the reduction temperatures are further decreased to values lower than what is found in pure GO.

The mechanism by which the VAc group promotes the reduction of GO is currently not known. However, work by T. Szabó et al. has shown that GO is slightly acidic, having a pH of 4.5 at 0.1 mg/mL.[61] This slight acidity may induce hydrolysis of vinyl acetate groups, creating alcohols on the polymer chains. Two papers by Dreyer et al., in 2010 and 2011, describe the ability of GO sheets to oxidize alcohols as well as unsaturated hydrocarbons to create aldehydes on the GO sheets as they oxidize alcohols and unsaturated hydrocarbons.[62,63] We suggest this as a likely mechanism by which the vinyl acetate groups enhance GO reduction. The vinylpyrrolidone groups do not have this ability; the polymer chemical structure in nanocomposites thus significantly affects the degree of *in situ* GO reduction.

In order to prove thermally induced *in situ* reduction of GO independently, electrical conductivity, optical absorption, and Raman spectroscopy measurements were performed. Heating of each of the composites was carried out using a temperature profile that matched the exothermic event in the DSC thermogram to establish the events' relation to GO reduction. The "onset" and "end" temperatures from Table 3 were used as starting and end points of a 1 °C/min temperature ramp.

The heated samples featured an increase in electrical conductivity with respect to the unheated samples by a factor of $2.2 \pm 0.2$ (GO–PVP), $2.0 \pm 0.3$ (GO–PVP/VAc), and $1.9 \pm 0.4$ (GO–PVAc). These increases are relatively moderate but clearly significant and thus a direct confirmation of GO reduction. Strong increases in conductivity have been reported for C:O ratios $\geq 10$;[13,23,24] a small increase in conductivity thus suggests that the C:O ratio in our case is lower. We currently do not know
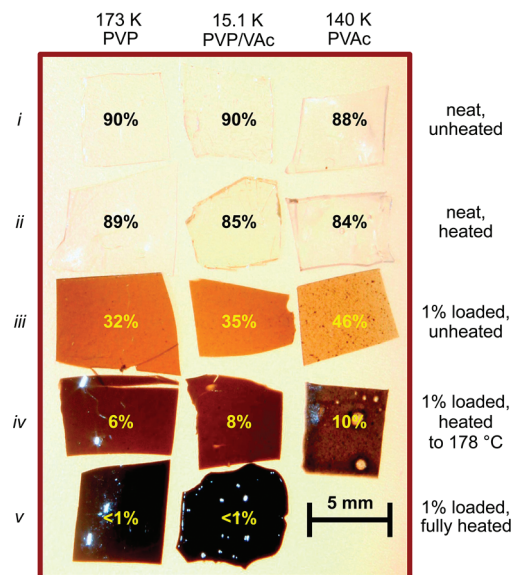


**Figure 9.** Photograph of the manufactured specimens to highlight changes in optical properties. Each of the three columns represents one of the polymers 173 K PVP, 15.1 K PVP/VAc, and 140 K PVAc. The five rows represent different GO loadings and processing conditions: (*i*) neat, (*ii*) neat, heated, (*iii*) loaded with 1% GO, (*iv*) loaded with 1% GO, heated to 178 °C, and (*v*) loaded with 1% GO and fully heated. Relative transmission of 633 nm light for the neat and GO-loaded polymers is added as overlaid black and yellow numbers, respectively.

the exact C:O ratios of the *in situ* reduced GO, since attempts of completely separating the polymer from the GO after heating for subsequent chemical analysis have proven unsuccessful. However, our results are in line with the relatively moderate C:O ratios of 4–8 we found in air and in DMF at similar temperatures (see Table 2).

The photograph in Figure 9 shows a series of specimens manufactured from each of the three different polymers—PVP, PVP/VAc, and PVAc—arranged in columns. Taken against a bright background, the picture illustrates the degree of optical absorption of each sample. Relative transmission of 633 nm laser light has been added as an overlay to each sample. The first row (*i*) shows the neat polymers; the second row (*ii*) features the pieces from the same samples made in the first row after heating. The difference in absorption of the samples is small: average transmission is reduced from about 90% to about 86%; the polymers alone thus do not undergo significant absorption changes upon heating. The nanocomposites containing 1% GO shown in the third row (*iii*) are darker due to the optical absorption caused by GO, with transmissions of ≈40% on average (the PVAc-based composite was thinnest and thus exhibited the greatest transmission). The degree of absorption was significantly increased when each of these samples was heated to a temperature of 178 °C (*iv*); average transmission was reduced to ≈8%. All composites underwent significant darkening with respect to their unheated counterparts (*iii*), which is a strong indicator for successful GO reduction.[49,64] For the PVAc-based composite, the temperature of 178 °C already represents the end point of the exothermic event; the other nanocomposite systems have higher end temperatures of their exothermic events (220 and 212 °C, respectively). Correspondingly, the PVAc-based sample features the greatest relative change in absorption. The last row (*v*), finally,
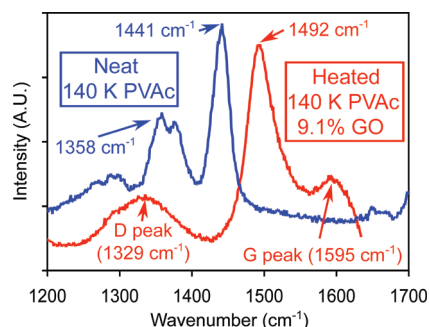
**Figure 10.** Raman spectra of neat 140 K PVAc (blue) and heated 9.1% GO−PVAc (red) composite. The neat material has characteristic peaks at 1358 and 1441 cm$^{-1}$. The reduced material exhibits a D peak at 1329 cm$^{-1}$ and a red-shifted G peak at 1595 cm$^{-1}$.
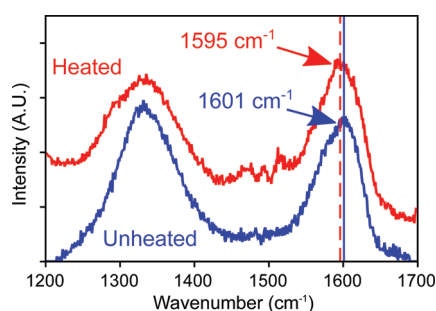


**Figure 11.** Raman spectra of unheated 9.1% GO−PVAc (blue) and heated (after subtraction of 1492 cm$^{-1}$ peak) GO−PVAc composites (red). The D peak of the unheated material is at 1332 cm$^{-1}$; the G peak is at 1601 cm$^{-1}$ (solid blue vertical line). The reduced material has a D peak at 1329 cm$^{-1}$ and a red-shifted G peak at 1595 cm$^{-1}$ (dotted red line).

shows PVP and PVP/VAc-based specimens after temperatures had been ramped to their end points; as expected, the absorption increased further, indicative of further reduction.[49,64] It is worth noting that the neat samples shown in the second row (*ii*) were heated to the same temperatures as the composites in the last row (*v*).

Raman spectra were taken from neat PVAc and from heated and unheated 9.1% GO−PVAc composites. The control spectrum taken from a neat 140 K PVAc sample (Figure 10) is in agreement with published PVAc spectra,[65] featuring distinct peaks at 1358 and 1441 cm$^{-1}$. The Raman spectrum of the unheated 9.1% GO−PVAc composite (Figure 11), is dominated by the two well-understood G and D peaks, which are found in all graphene-like systems. Polymer-related peaks are not significantly present in this spectrum. To determine the positions of the D and G peaks, a baseline was first subtracted;[66] more details are shown in the Supporting Information. The position of the D peak was 1332 cm$^{-1}$, determined by a Lorentzian fit.[67−69] The G peak was fit to a Breit−Wigner−Fano (BWF) equation due to its asymmetric shape;[67−69] the obtained peak position was 1601 cm$^{-1}$. This specific combination of fits for the D and G peaks is common in the literature.[69−78]

The Raman spectrum for the heated 9.1% GO−PVAc is shown in Figure 10. In contrast to the unheated composite, this spectrum shows a strong peak at 1492 cm$^{-1}$, which is neither present in the spectrum of the neat PVAc, nor in the GO

**Table 4. Raman D and G Peak Positions and Full-Width at Half-Maximum (FWHM) for Unheated and Heated 9.1% GO−PVAc Composites**

| material | D peak (Lorentzian fit) | | G peak (BWF fit) | |
|---|---|---|---|---|
| | position (cm$^{-1}$) | fwhm (cm$^{-1}$) | position (cm$^{-1}$) | fwhm (cm$^{-1}$) |
| GO−PVAc, unheated | 1332 | 87 | 1601 | 60 |
| GO−PVAc, heated | 1329 | 101 | 1595 | 80 |

spectrum. This peak is not known to occur in graphene-like materials and thus supports our hypothesis that the polymer is chemically altered during the GO reduction reaction. The heated composite still featured the D and G peaks due to GO; the D peak position was determined to be 1329 cm$^{-1}$. For increased accuracy in determining the position of the G peak, the neighboring 1492 cm$^{-1}$ peak (shown in Figure 10) was fitted by a Lorentzian and subtracted from the original spectrum. On the basis of the resulting spectrum (Figure 11) the G peak position was determined to be at 1595 cm$^{-1}$.

The D and G peak positions for unheated and heated GO−PVAc composites are summarized in Table 4; most notably, the G peak position was shifted by 6 cm$^{-1}$ from 1601 to 1595 cm$^{-1}$ by heating. This shift of the G peak[79] as well as its change in symmetry after heating is in line with the reduction of GO.[66] While Kudin et al. have reported a shift of 12 cm$^{-1}$ for near-complete reduction of GO to C:O ratios of up to 20, the smaller shift of 6 cm$^{-1}$ suggests a lesser degree of reduction.

## ■ CONCLUSION

The thermograms of all three neat polymers did not show any significant events in the investigated temperature range. When GO is added, a peak which is in line with thermally induced GO reduction appears on each of the composites' thermograms. The corresponding mass loss observed in the PVP−GO system is in excellent agreement with GO reduction. Several independent measurements confirmed the reduction of GO. The electrical conductivity was increased by a factor of ≈2 in all composite systems. This heat-induced increase in conductivity is mirrored by an increase in optical absorption after heating. Raman spectroscopy, finally, showed a red shift of the G peak by 6 cm$^{-1}$. The C:O ratio of our *in situ* reduced GO is currently not known. However, both the relatively small Raman peak shift and the very moderate increase of electrical conductivity after heating suggest a C:O ratio <10.[13,23,24]

The thermal data shows that the *in situ* reduction of GO in nanocomposites is significantly different for the three different polymer matrices. Incorporated into PVP, GO exhibited a lower heat of reduction than in air. In PVP/VAc, this stabilizing effect of PVP is countered by the presence of vinyl acetate groups, which promote GO reduction. Consequently, this promoting effect is even stronger when GO is embedded into pure PVAc, where significantly increased heats of reduction are observed. The corresponding shifts in the reaction temperatures mirror this situation. The implications, whether intended or unintended, of *in situ* GO reduction dependence on particle−polymer interaction are numerous. A change of the C:O ratio of GO during processing at moderate temperatures can lead to altered and/or unexpected changes in the macroscopic mechanical and electric properties of a nanocomposite. As an example, if there are

temperature gradients in thick composites during processing which produce variation in the C:O ratios with depth, this can result in variation in properties throughout the thickness.

In summary, we show that GO sheets in a polymer nanocomposite will be reduced to a higher C:O ratio depending on the time—temperature history at the particles' location and chemical structure of the surrounding polymer. This leads to changes in the particle—polymer interfacial forces and yields either improvement or reduction of desired mechanical properties of the polymer—GO nanocomposite. The electric and electronic properties of the nanocomposite are altered in a similar way.

## ■ ASSOCIATED CONTENT

**ⓢ Supporting Information.** Description of electrical conductivity measurements, including information on the sensor used, and more details on Raman data processing. This material is available free of charge via the Internet at http://pubs.acs.org.

## ■ ACKNOWLEDGMENT

## ■ REFERENCES

(1) Kim, H.; Abdala, A. A.; Macosko, C. W. *Macromolecules* **2010**, *43*, 6515–6530.

(2) Kim, H.; Miura, Y.; Macosko, C. W. *Chem. Mater.* **2010**, *22*, 3441–3450.

(3) Ramanathan, T.; Abdala, A. A.; Stankovich, S.; Dikin, D. A.; Herrera-Alonso, M.; Piner, R. D.; Adamson, D. H.; Schniepp, H. C.; Chen, X.; Ruoff, R. S.; Nguyen, S. T.; Aksay, I. A.; Prud'homme, R. K.; Brinson, L. C. *Nature Nanotechnol.* **2008**, *3*, 327–331.

(4) Stankovich, S.; Dikin, D. A.; Dommett, G. H. B.; Kohlhaas, K. M.; Zimney, E. J.; Stach, E. A.; Piner, R. D.; Nguyen, S. T.; Ruoff, R. S. *Nature* **2006**, *442*, 282–286.

(5) Lee, C.; Wei, X.; Kysar, J. W.; Hone, J. *Science* **2008**, *321*, 385–388.

(6) Du, X.; Skachko, I.; Barker, A.; Andrei, E. Y. *Nature Nanotechnol.* **2008**, *3*, 491–495.

(7) Bunch, J. S.; Verbridge, S. S.; Alden, J. S.; Van der Zande, A. M.; Parpia, J. M.; Craighead, H. G.; McEuen, P. L. *Nano Lett.* **2008**, *8*, 2458–2462.

(8) Fang, Z. H.; Punckt, C.; Leung, E. Y.; Schniepp, H. C.; Aksay, I. A. *Appl. Opt.* **2010**, *49*, 6689–6696.

(9) Cai, M.; Glover, A. J.; Wallin, T. J.; Kranbuehl, D. E.; Schniepp, H. C. *AIP Conf. Proc.* **2010**, *1255*, 95–97.

(10) Kranbuehl, D. E.; Cai, M.; Glover, A. J.; Schniepp, H. C. *J. Appl. Polym. Sci.* **2011**, *122*, 3740–3744.

(11) Schniepp, H. C.; Kudin, K. N.; Li, J.; Prud'homme, R. K.; Car, R.; Saville, D. A.; Aksay, I. A. *ACS Nano* **2008**, *2*, 2577–2584.

(12) Sundaram, R.; Gómez-Navarro, C.; Balasubramanian, K.; Burghard, M.; Kern, K. *Adv. Mater.* **2008**, *20*, 3050–3053.

(13) Schniepp, H.; Li, J.; McAllister, M.; Sai, H.; Herrera-Alonso, M.; Adamson, D. H.; Prud'homme, R. K.; Car, R.; Saville, D. A.; Aksay, I. A. *J. Phys. Chem. C* **2006**, *110*, 8535–8539.

(14) Hummers, W. S., Jr.; Offeman, R. E. *J. Am. Chem. Soc.* **1958**, *80*, 1339–1339.

(15) Stankovich, S.; Dikin, D. A.; Piner, R. D.; Kohlhaas, K. A.; Kleinhammes, A.; Jia, Y.; Wu, Y.; Nguyen, S. T.; Ruoff, R. S. *Carbon* **2007**, *45*, 1558–1565.

(16) McAllister, M.; Li, J.; Adamson, D.; Schniepp, H.; Abdala, A.; Liu, J.; Herrera-Alonso, M.; Milius, D. L.; Car, R.; Prud'homme, R. K.; Aksay, I. A. *Chem. Mater.* **2007**, *19*, 4396–4404.

(17) Lerf, A.; He, H.; Forster, M.; Klinowski, J. *J. Phys. Chem. B* **1998**, *102*, 4477–4482.

(18) Park, S.; An, J.; Jung, I.; Piner, R. D.; An, S. J.; Li, X.; Velamakanni, A.; Ruoff, R. S. *Nano Lett.* **2009**, *9*, 1593–1597.

(19) Pham, V. H.; Cuong, T. V.; Hur, S. H.; Oh, E.; Kim, E. J.; Shin, E. W.; Chung, J. S. *J. Mater. Chem.* **2011**, *21*, 3371–3377.

(20) Dubin, S.; Gilje, S.; Wang, K.; Tung, C. V.; Cha, K.; Hall, A. S.; Farrar, J.; Varshneya, R.; Yang, Y.; Kaner, R. B. *ACS Nano* **2010**, *4*, 3845–3852.

(21) Bonaccorso, F.; Su, Z.; Hasan, T.; Ferrari, A. C. *Nat. Photonics* **2010**, *4*, 611–622.

(22) Luo, Z.; Vora, P. M.; Mele, E. J.; Johnson, A. T. C.; Kikkawa, J. M. *Appl. Phys. Lett.* **2009**, *94* (111909), 1–3.

(23) Park, S.; Ruoff, R. S. *Nat. Nanotechnol.* **2009**, *4*, 217–224.

(24) Compton, O. C.; Jain, B.; Dikin, D. A.; Abouimrane, A.; Amine, K.; Nguyen, S. T. *ACS Nano* **2011**, *5*, 4380–4391.

(25) Wei, Z.; Wang, D.; Kim, S.; Kim, S.; Hu, Y.; Yakes, M. K.; Laracuente, A. R.; Dai, Z.; Marder, S. R.; Berger, C.; King, W. P.; De Heer, W. A.; Sheehan, P. E. *Science* **2010**, *328*, 1373–1376.

(26) Cao, Y.; Feng, J.; Wu, P. *Carbon* **2010**, *48*, 3834–3839.

(27) Gilje, S.; Han, S.; Wang, M.; Wang, K. L.; Kaner, R. B. *Nano Lett.* **2007**, *7*, 3394–3398.

(28) Gómez-Navarro, C.; Meyer, J. C.; Sundaram, R. S.; Chuvilin, A.; Kurasch, S.; Burghard, M.; Kern, K.; Kaiser, U. *Nano Lett.* **2010**, *10*, 1144–1148.

(29) Gómez-Navarro, C.; Weitz, R. T.; Bittner, A. M.; Scolari, M.; Mews, A.; Burghard, M.; Kern, K. *Nano Lett.* **2007**, *7*, 3499–3503.

(30) Jiang, L.; Shen, X.; Wu, J.; Shen, K. *J. Appl. Polym. Sci.* **2010**, *118*, 275–279.

(31) Lee, S.; Lim, S.; Lim, E.; Lee, K. L. *J. Phys. Chem. Solids* **2010**, *71*, 483–486.

(32) Stankovich, S.; Piner, R. D.; Chen, X.; Wu, N.; Nguyen, S. T.; Ruoff, R. S. *J. Mater. Chem.* **2006**, *16*, 155–158.

(33) Tung, V. C.; Allen, M. J.; Yang, Y.; Kaner, R. B. *Nat. Nanotechnol.* **2009**, *4*, 25–29.

(34) Watcharotone, S.; Dikin, D. A.; Stankovich, S.; Piner, R.; Jung, I.; Dommett, G. H. B.; Evmenenko, G.; Wu, S.; Chen, S.; Liu, C.; Nguyen, S. T.; Ruoff, R. S. *Nano Lett.* **2007**, *7*, 1888–1892.

(35) Shin, H.; Kim, K. K.; Benayad, A.; Yoon, S.; Park, H. K.; Jung, I.; Jin, M. H.; Jeong, H.; Kim, J. M.; Choi, J.; Lee, Y. H. *Adv. Funct. Mater.* **2009**, *19*, 1987–1992.

(36) Wang, G.; Yang, J.; Park, J.; Gou, X.; Wang, B.; Liu, H.; Yao, J. *J. Phys. Chem. C* **2008**, *112*, 8192–8195.

(37) Fan, X.; Peng, W.; Li, X.; Wang, S.; Zhang, G.; Zhang, F. *Adv. Mater.* **2008**, *20*, 4490–4493.

(38) Zhang, Jiali; Yang, H.; Shen, G.; Cheng, P.; Zhang, J.; Guo, S. *Chem. Commun.* **2010**, *46*, 1112–1114.

(39) Fernández-Merino, M. J.; Guardia, L.; Paredes, J. I.; Villar-Rodil, S.; Solís-Fernández, P.; Tascon, J. M. D. *J. Phys. Chem. C* **2010**, *114*, 6426–6432.

(40) Liu, Jincheng; Jeong, H.; Liu, Jinzhang; Lee, K.; Park, J.; Ahn, Y. H.; Lee, S. *Carbon* **2010**, *48*, 2282–2289.

(41) Zhu, C.; Guo, S.; Fang, Y.; Dong, S. *ACS Nano* **2010**, *4*, 2429–2437.

(42) Liu, J.; Fu, S.; Yuan, B.; Li, Y.; Deng, Z. *J. Am. Chem. Soc.* **2010**, *132*, 7279–7281.

(43) Fan, Z.; Wang, K.; Wei, T.; Yan, J.; Song, L.; et al. *Carbon* **2010**, *48*, 1670–1692.

(44) Wu, Z.; Ren, W.; Gao, L.; Liu, B.; Jiang, C.; et al. *Carbon* **2009**, *47*, 493–499.

(45) Wang, X.; Zhi, L.; Müllen, K. *Nano Lett.* **2008**, *8*, 323–327.

(46) Jung, I.; Field, D.; Clark, N.; Zhu, Y.; Yang, D.; Piner, R. D.; Stankovich, S.; Dikin, D. A.; Geisler, H.; Ventrice, C. A., Jr.; Ruoff, R. S. *J. Phys. Chem. C* **2009**, *113*, 18480–18486.

(47) Cuong, T. V.; Pham, V. H.; Tran, Q. T.; Chung, J. S.; Shin, E. W.; Kim, J. S.; Kim, E. J. *Mater. Lett.* **2010**, *64*, 765–767.

(48) Li, X.; Wang, H.; Robinson, J.; Sanchez, H.; Diankov, G.; Dai, H. *J. Am. Chem. Soc.* **2009**, *131*, 15939–15944.

(49) Cote, L. J.; Cruz-Silva, R.; Huang, J. *J. Am. Chem. Soc.* **2009**, *131*, 11027–11032.

(50) Williams, G.; Seger, B.; Kamat, P. V. *ACS Nano* **2008**, *2*, 1487–1491.

(51) Liao, K.; Mittal, A.; Bose, S.; Leighton, C.; Mkhoyan, K. A.; Macosko, C. W. *ACS Nano* **2011**, *5*, 1253–1258.

(52) Nethravathi, C.; Rajamathi, M. *Carbon* **2008**, *46*, 1994–1998.

(53) Chen, W.; Yan, L. *Nanoscale* **2010**, *2*, 559–563.

(54) Chen, W.; Yan, L.; Bangal, P. R. *Carbon* **2010**, *48*, 1146–1152.

(55) Zhou, Y.; Bao, Q.; Tang, L. A. L.; Zhong, Y.; Loh, K. P. *Chem. Mater.* **2009**, *21*, 2950–2956.

(56) Zhu, Y.; Stoller, M. D.; Cai, W.; Velamakanni, A.; Piner, R. D.; Chen, D.; Ruoff, R. S. *ACS Nano* **2010**, *2*, 1227–1233.

(57) Lin, Z.; Yao, Y.; Li, Z.; Liu, Y.; Li, Z.; Wong, C. *J. Phys. Chem. C* **2010**, *114*, 14819–14825.

(58) Swei, J.; Talbot, J. B. *J. Appl. Polym. Sci.* **2003**, *90*, 1153–1155.

(59) *International Specialty Products, Polyvinylpyrrolidone Polymers, product brochure*; International Specialty Products: Wayne, NJ.

(60) *International Specialty Products, Polyvinylpyrrolidone/Polyvinyl Acetate Copolymers, product brochure*; International Specialty Products: Wayne, NJ.

(61) Szabó, T.; Tombácz, E.; Illés, E.; Dékány, I. *Carbon* **2006**, *44*, 537–538.

(62) Dreyer, D.; Jia, H.; Bielawski, C. *Angew. Chem., Int. Ed.* **2010**, *49*, 6813–6816.

(63) Dreyer, D.; Murali, S.; Zhu, Y.; Ruoff, R.; Bielawski, C. *J. Mater. Chem.* **2011**, *21*, 3443–3447.

(64) Zhou, Y.; Bao, Q.; Tang, L. A. L.; Zhong, Y.; Loh, K. P. *Chem. Mater.* **2009**, *21*, 2950–2956.

(65) Lobo, H.; Bonilla, J. *Handbook of Plastics Analysis*: Marcel Dekker: New York, 2003; Vols. 236–240, p 315.

(66) Kudin, K.; Ozbas, B.; Schniepp, H.; Prud'homme, R.; Aksay, I.; Car, R. *Nano Lett.* **2008**, *8*, 36–41.

(67) Ferrari, A.; Robertson, J. *Phys. Rev. B* **2000**, *51*, 14095–14107.

(68) Robertson, J. *Mater. Sci. Eng. R* **2002**, *37*, 129–281.

(69) Tai, F.; Lee, S.; Chen, J.; Wei, C.; Chang, S. *J. Raman Spectrosc.* **2009**, *40*, 1055–1059.

(70) Prawer, S.; Nugent, K.; Lifshitz, Y.; Lempert, G.; Grossman, E.; Kulik, J.; Avigal, I.; Kalish, R. *Diamond Relat. Mater.* **1996**, *5*, 433–438.

(71) Xu, S.; Flynn, D.; Tay, B.; Prawer, S.; Nugent, K.; Silva, S.; Lifshitz, Y.; Milne, W. *Philos. Mag. B* **1997**, *76*, 351–361.

(72) Gilkes, K.; Prawer, S.; Nugent, K.; Robertson, J.; Sands, H.; Lifshitz, Y.; Xu, S. *J. Appl. Phys.* **2000**, *87*, 7283–7289.

(73) McCulloch, D.; Prawer, S.; Hoffman, A. *Phys. Rev. B* **1994**, *50*, 5905–5917.

(74) McCulloch, D.; Prawer, S. *J. Appl. Phys.* **1995**, *78*, 3040–3047.

(75) Kleinsorge, B.; Rodil, S.; Adamopoulos, G.; Robertson, J.; Grambole, D.; Fukarek, W. *Diamond Relat. Mater.* **2001**, *10*, 965–969.

(76) Ferrari, A.; Rodil, S.; Robertson, J. *Diamond Relat. Mater.* **2003**, *12*, 905–910.

(77) Ferrari, A.; Robertson, J. *Phys. Rev. B* **2001**, *64*, 075414/1–075414/13.

(78) Nakazawa, H.; Mikami, T.; Enta, Y.; Suemitsu, M.; Mashita, M. *Jpn. Appl. Phys.* **2003**, *42*, L676–L679.

(79) Tuinstra, R.; Koenig, J. *J. Chem. Phys.* **1970**, *53*, 1126–1130.